*Vietnam Journal of Science and Technology* ***64***(1) (2026) 175–188
DOI: https://doi.org/10.15625/2525-2518/22041

# Concept and optimization of SMA dampers to control the first three natural vibration modes in cable-stayed bridges

**Hoang Ngoc Quy[1,2], Nguyen Van Duy[2], TruongGiang Nguyen[1,3,*]**

[1]*Institute of Mechanics, Vietnam Academy of Science and Technology, 18 Hoang Quoc Viet, Nghia Do, Ha Noi, Viet Nam*
[2]*Faculty of Civil Engineering, VNU University of Engineering and Technology, 144 Xuan Thuy, Cau Giay, Ha Noi, Viet Nam*
[3]*Faculty of Engineering Mechanics and Automation, VNU University of Engineering and Technology,144 Xuan Thuy, Cau Giay, Ha Noi, Viet Nam*

[*]Email: *ntgiang@imech.vast.vn*

Received: 05 December 2024; Accepted for publication: 16 June 2025

**Abstract.** Cable-stayed bridges are often subjected to cable vibrations caused by wind, traffic, and other dynamic loads, which can significantly reduce their structural lifespan. To address this issue, our study proposes a two-floor damping design that leverages the superelasticity and superior energy dissipation capabilities of shape memory alloys (SMA). A simplified constitutive model was developed to simulate the superelastic behavior of SMA, optimizing critical parameters such as length, diameter, and installation position on cable-stayed bridges. Through simulations and dynamic response analysis, the SMA damper demonstrated exceptional effectiveness in dissipating energy across various vibration modes, significantly enhancing structural stability. Furthermore, this paper highlights the advantages of the two-floor SMA damper in mitigating cable vibrations under diverse oscillation modes and identifies an optimal set of parameters for practical installation, contributing to cost efficiency and extended bridge lifespan. A comparison with the results of tuned mass damper (TMD) device is also carried out to evaluate the damping efficiency of the SMA device.

*Keywords:* shape memory alloy, martensitic phase transformation, superelastic, vibration, damper.

*Classification number:* 5.4.5.

## 1. INTRODUCTION

Cable-stayed bridges are widely used due to their aesthetics, long spans, and construction efficiency, but they are prone to cable vibrations induced by wind, traffic, and other dynamic loads, which can cause fatigue and shorten service life [1, 2]. Conventional passive control solutions, including tuned mass dampers, friction dampers, viscous dampers, and fluid-based systems, have been applied to mitigate these vibrations; however, their effectiveness may be limited and maintenance can be challenging [3–5].

In recent years, shape memory alloys have emerged as a potential solution for vibration control due to their unique superelastic properties and their ability to absorb and dissipate energy. SMA materials, particularly nickel-titanium (NiTi) alloys, exhibit significant hysteresis and can withstand large deformations while returning to their original shape, making them ideal for damping applications [6-9]. Research has shown that using SMAs in damping systems can significantly improve the performance of cable-stayed bridges, reducing harmful vibrations and extending the bridge's lifespan [10, 11]. One of the main advantages of SMAs is their exceptional flexibility, allowing them to function effectively in a wide range of environmental conditions. By adjusting the quantity and/or characteristics of the SMA components, it is possible to optimize their energy dissipation capabilities, thereby enhancing damping efficiency. Furthermore, SMAs exhibit excellent fatigue resistance under large deformation cycles and ensure high durability and reliability over long periods of use. These properties are particularly important for cable-stayed bridges, where weather conditions can change rapidly and lead to unpredictable dynamic loads [12]. The superelastic properties of SMAs allow them to absorb and dissipate large amounts of energy from vibrations, mitigating negative impacts on the bridge structure [13, 14]. SMA dampers, such as the proposed SMAS-TMD with pre-tensioned SMA helical springs [9], have shown superior vibration reduction capabilities compared to traditional dampers. Additionally, the use of SMA dampers can effectively prevent the common detuning phenomena observed in optimally tuned mass dampers [15].

This paper presents the design, site survey, and performance evaluation of SMA dampers developed for cable-stayed bridges. Key design parameters, including the optimal length and diameter of SMA wires, are investigated to maximize damping efficiency, while a site survey is conducted to determine suitable installation locations for practical application. To support the design process, a simplified simulation model is proposed to capture the superelastic behavior of SMA materials, enabling efficient optimization with straightforward solution procedures. In addition, the dynamic response of stay cables is examined under multiple natural vibration modes to better evaluate the damper performance under different oscillation conditions. The paper is organized as follows: Section 2 introduces the two-floor SMA damper concept and its design features; Section 3 presents the simplified SMA constitutive model and the governing dynamic equations of inclined cables with damper forces included; Section 4 compares numerical results with a tuned mass damper (TMD) and optimizes the SMA damper parameters (area, length, and position); and Section 5 summarizes the main conclusions.

## 2. CONCEPT OF SMA DAMPER

In this concept, we aim to present a two-floor SMA damper with high energy dissipation capacity and complete deformation recovery. A central plate is directly connected to the cable-stayed cables, ensuring that the SMA wires operate under alternating tension as the cables vibrate. The SMA wires are arranged at the four corners of a square layout, providing enhanced stability for the device. This damper is specially optimized to reduce vibrations in the cables of cable-stayed bridges by utilizing shape memory alloy wires, known for their unique superelastic properties. These properties enable efficient energy absorption and recovery after repeated cycles of deformation. The prototype of the SMA damper, shown in Figure 1, consists of three main parts:

*Connection system to the bridge:*

This system secures the damper to the bridge structure. The connection ensures that the damper remains stable and can effectively transmit forces from the vibrating cables to the SMA wires.

*Central plate moving with the cable-stayed cables:*

The central plate is designed to move synchronously with the cable-stayed cables. This plate transfers the vibrational forces from the cables to the SMA wires, ensuring efficient energy absorption by the SMA wires.

*Connection system to the cable-stayed cables*:

This system links the damper directly to the cable-stayed cables. The robust connection allows the damper to absorb and dissipate the vibrational energy transmitted through the cables.

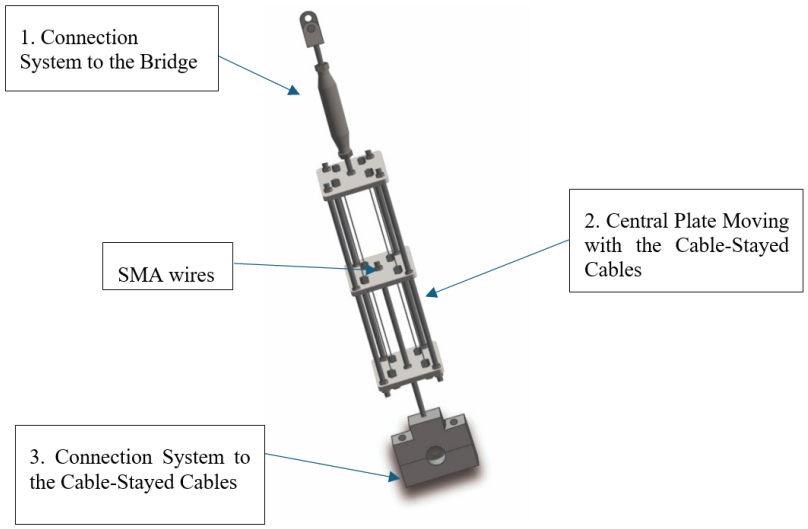


*Figure 1.* Overall concept of a two-stage damper using shape memory alloy materials.

The SMA wires play a crucial role in the damper, serving as the core component that maximizes the device's energy dissipation efficiency. With a smart concept that incorporates four wires within the structure, the SMA wires are capable of evenly absorbing and distributing vibrational energy. Made from nickel-titanium alloy, known for its exceptional strength and fatigue resistance, the SMA wires ensure efficient performance through repeated cycles of mechanical loading and unloading. This concept not only significantly reduces harmful vibrations but also extends the lifespan of cable-stayed bridges. The strategic arrangement and unique shape-memory properties of the SMA wires ensure that the damper operates reliably and stably, making it an ideal solution for vibration control in modern bridge engineering.

## 3. BASIC EQUATIONS

### 3.1. Constitutive model for superelastic shape memory alloys

#### *3.1.1. Free energy*

In the one-dimensional (1D) model of SMA, the thermo-mechanical behavior is characterized by a trio of variables: total strain ($\varepsilon$), temperature ($T$), and the martensite fraction

$(z)$. Here, $\varepsilon$ represents the deformation experienced by the material, $T$ indicates the operational temperature, and $z$ denotes the proportion of the martensitic phase within the alloy. The martensite fraction $z$ ranges from 0 to 1, where $z = 0$ signifies that the material is entirely in the austenitic phase, and $z = 1$ indicates a fully martensitic phase. This modeling approach provides a simplified yet effective means to describe the phase transformation behavior and the corresponding mechanical response of SMAs under various thermal and mechanical loads, facilitating the concept and optimization of SMA-based devices. The Helmholtz free energy density which depends on state variables and internal variables is chosen as:

$$W = W(\varepsilon, T, z) \tag{1}$$

Based on the work by Hoang *et al.* [16], we propose that the Helmholtz free energy (per unit volume) under isothermal conditions is defined by the following function:

$$W(\varepsilon, \varepsilon^{in}, z) = \frac{1}{2}\left(1 - z + \tau\right)E\left(\varepsilon - \varepsilon^{in}\right)^2 + f(z) \tag{2}$$

where $E$ is the elastic modulus, $\tau$ is a constant and $\varepsilon^{in}$ represents the inelastic strain. The hardening function is designed to capture the interactions between the austenitic and martensitic phases, as well as the interactions among the different martensitic variants. This function, $f(z)$, takes the following form during both the forward and reverse phase transformations:

$$f(z) = \begin{cases} \frac{1}{2}Hz^2 + \frac{1}{2}Gz, & \dot{z} > 0 \\ \frac{1}{2}Hz^2 + \frac{1}{2}Iz, & \dot{z} < 0 \end{cases} \tag{3}$$

where $H, G$, and $I$ are constant material parameters.

### *3.1.2. Evolution of internal state variables*

The Clausius-Duhem inequality can be expressed as:

$$\left(\sigma - \frac{\partial W}{\partial \varepsilon}\right)\dot{\varepsilon} + \left(-\frac{\partial W}{\partial \varepsilon^{in}}\right)\dot{\varepsilon}^{in} + \left(-\frac{\partial W}{\partial z}\right)\dot{z} \geq 0 \tag{4}$$

A sufficient condition for inequality (4) to be satisfied for any $\dot{\varepsilon}$ is that the respective coefficients must be zero, thus yielding:

$$\sigma = \frac{\partial W}{\partial \varepsilon} = (1 - z + \tau)E(\varepsilon - \varepsilon^{in}) \tag{5}$$

Now that we have identified the set of internal state variables $\varepsilon^{in}$ and $z$, we need to determine the evolution equations for these internal state variables. The Clausius-Planck inequality can be expressed as follows:

$$\left(-\frac{\partial W}{\partial \varepsilon^{in}}\right)\dot{\varepsilon}^{in} + \left(-\frac{\partial W}{\partial \xi}\right)\dot{z} \geq 0 \tag{6}$$

By substituting Eq. (2) into Eq. (6), we obtain:

$$(1 - z + \tau)E\left(\varepsilon - \varepsilon^{in}\right)\dot{\varepsilon}^{in} - \left(-\frac{1}{2}E\left(\varepsilon - \varepsilon^{in}\right)^2 + \frac{\partial f(z)}{\partial z}\right)\dot{z} \geq 0 \tag{7}$$

The inelastic strain, $\varepsilon^{in}$, depends on the martensite fraction $z$ [17]:

$$\varepsilon^{in} = \varepsilon_L z \, \mathrm{sgn}(\sigma) \tag{8}$$

$\varepsilon_L$ is the maximum residual strain, sgn(•) is the sign function, and $\sigma$ is the uniaxial stress. From Eq. (8) and substituting Eq. (7), we derive:

$$\left(\sigma\varepsilon_L sgn(\sigma) + \frac{1}{2}E(\varepsilon - \varepsilon_L z sgn(\sigma))^2 - \frac{\partial f(z)}{\partial z}\right)\dot{z} = \Phi\dot{z} \geq 0 \tag{9}$$

where $\Phi$ is defined as above and represents the general thermodynamic force conjugate to $z$. For the Helmholtz free energy by Eq. (2), the explicit form of $\Phi$ is:

$$\Phi(\varepsilon, z) = \sigma\varepsilon_L sgn(\sigma) + \frac{1}{2}E(\varepsilon - \varepsilon_L z sgn(\sigma))^2 - \frac{\partial f(z)}{\partial z} \tag{10}$$

we consider uniaxial tension so $sgn(\sigma) = +1$. To complete the model, the rate-independent dissipation potential is formulated as follows:

$$D(\dot{z}) = \Phi_c\dot{z} \text{ with } \Phi_c > 0 \tag{11}$$

It is necessary to establish the conditions under which martensitic phase transformations, both forward and reverse, occur. The constitutive model provided posits that these transformations happen when the thermodynamic force $\Phi$ attains a critical threshold. This assumption must be incorporated to ensure that the Clausius-Planck inequality holds true for all potential thermomechanical trajectories.

When the forward martensitic transformation occurs, $\dot{z}$ takes positive values because austenite is transforming into martensite. Hence, for the Clausius-Planck inequality (9) to hold, $\Phi$ must be positive. Thus, during the forward transformation $\dot{z} > 0$, the function $\Phi$ reaches the threshold value:

$$\Phi = \frac{\partial D(\dot{z})}{\partial \dot{z}} = \Phi_c \tag{12}$$

where

$$\Phi_c = \sigma_s^{AM}\varepsilon_L \tag{13}$$

and $\sigma_s^{AM}$ is the stress that starts the phase transformation from austenite to martensite.

Conversely, during the reverse martensitic transformation, $\dot{z}$ is negative as martensite reverts to austenite. For the Clausius-Planck inequality (9) to be satisfied, $\Phi$ must be negative. Therefore, during the reverse transformation $\dot{z} < 0$, the function $\Phi$ becomes:

$$\Phi = -\frac{\partial D(\dot{z})}{\partial \dot{z}} = -\Phi_c \tag{14}$$

where

$$\Phi_c = \sigma_s^{MA}\varepsilon_L \tag{15}$$

and $\sigma_s^{MA}$ is the stress that starts the phase transformation from martensite to austenite. Finally, when the SMA is in a state where no phase transformation occurs, $\dot{z} = 0$, meaning $z$ remains constant. In this scenario, the Clausius-Planck inequality is automatically satisfied because $\Phi\dot{z} = 0$. The criteria for both forward and reverse martensitic transformations can be encapsulated by introducing a transformation function $f(\varepsilon, z)$, such that:

$$\begin{cases} f(\varepsilon, z) = \Phi - \Phi_c \leq 0; & f(\varepsilon, z)\dot{z} = 0; \quad \text{whenever } \dot{z} \geq 0 \\ f(\varepsilon, z) = -\Phi - \Phi_c \leq 0; & f(\varepsilon, z)\dot{z} = 0\,; \quad \text{whenever } \dot{z} \leq 0 \end{cases} \tag{16}$$

Substituting relation (10) into Eq. (16) results in two quadratic equations:

$$A_1 z^2 + B_1 z + C_1 = 0 \quad \text{whenever } \dot{z} > 0 \tag{17}$$

$$A_2 z^2 + B_2 z + C_2 = 0 \quad \text{whenever } \dot{z} < 0 \tag{18}$$

The coefficients for these quadratic equations are determined as follows:

$$A_1 = \frac{3}{2}E\varepsilon_L^2 \tag{19}$$

$$B_1 = -H - E\varepsilon_L^2 - 2E\varepsilon_L\varepsilon - E\varepsilon_L^2\tau \tag{20}$$

$$C_1 = \frac{1}{2}E\varepsilon^2 + \varepsilon(E\varepsilon_L + E\varepsilon_L\tau) - \sigma_s^{AM}\varepsilon_L - \frac{G}{2} \tag{21}$$

$$A_2 = \frac{3}{2}E\varepsilon_L^2 \tag{22}$$

$$B_2 = -H - L\varepsilon_L^2 - 2E\varepsilon_L\varepsilon - E\varepsilon_L^2\tau \tag{23}$$

$$C_2 = \frac{1}{2}E\varepsilon^2 + \varepsilon(E\varepsilon_L + E\varepsilon_L\tau) - \sigma_s^{MA}\varepsilon_L - \frac{I}{2} \tag{24}$$

The solutions can be found by solving quadratic equations (17) and (18).

### 3.2. Dynamic equations formulation of a sag stay cable

We begin by examining a cable connecting two points, $A$ and $B$, separated by a distance $L$ and forming an angle $\theta$ with the horizontal axis. Considering only the cable's self-weight, this structure remains stable in the plane, with the orthogonal reference system in this plane denoted as $Axy$. In this plane, the cable can oscillate along the $Oy$ direction (Figure 2(a)), while out-of-plane oscillations occur along the $Az$ direction, forming the orthogonal frame $Axyz$ [18, 19]. The cable's free vibration modes include the first, second, and third modes, illustrated in Figure 2(b). The SMA damper, installed at position $x_c$, generates a force $f_c$ applied to the cable, helping to control and reduce vibrations under various load conditions.

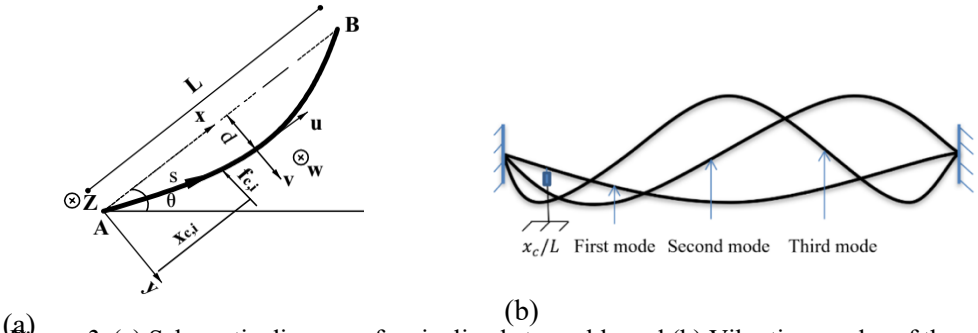


(a) (b)

*Figure 2.* (a) Schematic diagram of an inclined stay cable and (b) Vibration modes of the cable.

The partial differential equations governing this equilibrium, while accounting for the influence of an SMA damper, can be expressed as follows [20]:

$$\begin{cases} \dfrac{\partial}{\partial s}\left[(T+\tau)\left(\dfrac{dx}{ds}+\dfrac{\partial u}{\partial s}\right)\right] + F_x(x,t) = m\dfrac{\partial^2 u}{\partial t^2} - mg\sin\theta \\ \dfrac{\partial}{\partial s}\left[(T+\tau)\left(\dfrac{dy}{ds}+\dfrac{\partial v}{\partial s}\right)\right] + F_y(x,t) - \displaystyle\sum_{i=1}^{M} f_{c,i}(t)\,\delta\left(x-x_{c,i}\right) = m\dfrac{\partial^2 v}{\partial t^2} - mg\cos\theta \\ \dfrac{\partial}{\partial s}\left[(T+\tau)\dfrac{\partial w}{\partial s}\right] + F_z(x,t) = m\dfrac{\partial^2 w}{\partial t^2} \end{cases} \tag{25}$$

where $T$ is the static cable tension, $\tau$ is is the dynamic cable tension, $t$ is the time, $\delta$ is the Dirac delta function, and $u, v, w$ are the displacement components of the cable in the $x, y$ and $z$ directions, respectively, measured from the equilibrium position of the static cable. $F_x, F_y$ and $F_z$ are the distributed dynamic external loads per unit length in the $x, y$ and $z$ directions, and $f_{c,i}$ represents the force exerted by the damper on the cable at position $x_{c,i}$. The Dirac delta function $\delta(x - x_{c,i})$ is used to model the pointwise application of damper forces. The parameter $M$ indicates the total number of SMA dampers installed along the cable. This formulation is consistent with previous studies on coupled dynamic systems with discrete nonlinear damping mechanisms.

To derive the governing equation, the original non-linear equations are simplified using the following key assumptions: the cable's transverse frequency is lower than its longitudinal frequency, vibrations are limited to the $xy$-plane with negligible movement in the $x$-direction, the static cable shape is approximated as a parabola, and the sag-to-span ratio is small enough to be ignored. These assumptions were proposed in the research by Soltane *et al.* [21]. The study focuses on the free vibration response of the cable, as initial impulses from wind-induced excitations lead to natural mode vibrations.

As the analysis is restricted to transverse vibrations, we retain only the second equation from the equilibrium system (25), which governs the displacement component $v$ in the $y$-direction. The transverse deflection can be represented by a finite sum of modes, expressed as:

$$v = \sum_{i=1}^{N} \alpha_i(t)\varphi_i(x) \tag{26}$$

where, $\alpha_i(t)$ represents the dimensionless mode coefficients, and $\varphi_i(x)$ is a set of mode shape functions assumed to be continuous and satisfying the geometric boundary conditions $\varphi_i(0) = \varphi_i(L) = 0$. To calculate the damping effectiveness of the SMA damper, we assume $\varphi_i(x) = sin\left(\frac{i\pi x}{L}\right)$ with $i$ is the mode number. Based on the assumptions in Fugazza [22], we focus on the second equation in system (25), which governs the transverse vibration in the $y$-direction and includes the localized forces exerted by the SMA dampers. By multiplying both sides of the equation by $\varphi_j(x)$ and integrating over the length of the cable from 0 to $L$, we obtain a general form equation:

$$\begin{aligned} \int_0^L m\frac{\partial^2 v}{\partial t^2}\varphi_j(x)dx - \int_0^L T\frac{\partial^2 v}{x^2}\varphi_j(x)dx + \lambda^2 \int_0^L \int_0^L v(x,t)\varphi_j(x)dx \\ = \int_0^L \left( F_y(x,t) - \sum_{i=1}^{M} f_{c,i}(t)\,\delta(x - x_{c,i}) \right)\varphi_j(x)dx \end{aligned} \tag{27}$$

Substituting Eq. (26) into Eq. (27), we obtain:

$$\sum_{i=1}^{N}\left[m\ddot{\alpha}_i(t)\int_0^L \varphi_i(x)\,\varphi_j(x)dx - T\alpha_i(t)\int_0^L \varphi_i''(x)\,\varphi_j(x)dx + \lambda^2\alpha_i(t)\int_0^L \varphi_i(x)dx\int_0^L \varphi_j(x)dx\right] = \int_0^L\left(F_y(x,t) - \sum_{i=1}^{M} f_{c,i}(t)\,\delta\big(x - x_{c,i}\big)\right)\varphi_j(x)dx \tag{28}$$

Due to orthogonality, the inner products $\int_0^L \varphi_i(x)\,\varphi_j(x)$ and $\int_0^L \varphi_i''(x)\,\varphi_i(x)$ vanish for $i \neq j$, resulting in a decoupled equation for each mode $i$. After simplification, we obtain:

$$m\ddot{\alpha}_i(t)\int_0^L \varphi_i(x)\,\varphi_i(x)dx - T\alpha_i(t)\int_0^L \varphi_i''(x)\,\varphi_i(x)dx + \lambda^2\alpha_i(t)\int_0^L \varphi_i(x)dx\int_0^L \varphi_i(x)dx = F_{yi} - f_c(t)\varphi_i(x_c) \tag{29}$$

This expression is then simplified by integrating by parts and applying the boundary conditions. Consequently, the modal coefficients $\alpha_i(t)$ must satisfy the following second-order differential equation:

$$m_{ii}\ddot{\alpha}_i(t) + k_{ii}\alpha_i(t) = F_{yi} - f_c(t)\varphi_i(x_c) \tag{30}$$

where:

$$\begin{cases} \lambda^2 = \dfrac{EA}{L}\left(\dfrac{mg\cos\theta}{T}\right)^2 \\ m_{ii} = m\displaystyle\int_0^L \varphi_i(x)\varphi_i(x)\,dx = m\frac{L}{2} \\ k_{ii} = -T\displaystyle\int_0^L \varphi_i''(x)\varphi_i(x)dx + \lambda^2\int_0^L \varphi_i(x)dx\int_0^L \varphi_i(x)dx = \dfrac{T\pi^2 i^2}{2L} + \lambda^2\dfrac{4L^2}{i^2\pi^2} \\ F_{yi} = \displaystyle\int_0^L F_y(x,t)\varphi_i(x)dx \\ \varphi_i(x_c) = sin\left(\dfrac{i\pi x_c}{L}\right) \end{cases} \tag{31}$$

Eq. (30) captures the essential dynamics of the system, including the mass, stiffness, and damping effects of the cable, as well as the external forces and the influence of the SMA damper. The system of dynamical equations is decoupled in all terms except for the term $f_c$, which is introduced by the presence of the SMA damper. This SMA damper introduces non-linearity into the otherwise linear cable-damper system. To compute the dynamic response of the cable, the Newmark numerical method is used. The damping force $f_c$ will clearly depend on the constitutive behavior of the SMA.

## 4. OPTIMIZATION OF THE CROSS-SECTIONAL AREA, LENGTH OF SMA WIRES, AND POSITION OF THE SMA DAMPER

To optimize SMA parameters such as wire cross-sectional area and length, the energy method is commonly adopted to ensure maximum damping efficiency [18, 21]. The SMA performs optimally when it dissipates the maximum possible energy of the structural system. For a single vibration mode, the energy balance of equation (30) is expressed as:

$$E_k(t) + E_e(t) = E_i(t) + E_c(t) \tag{32}$$

where $E_k(t) = \frac{1}{2} m_{ii} \dot{\alpha}_i^2(t)$ and $E_e(t) = \frac{1}{2} k_{ii} \alpha_i^2(t)$ are the kinetic and elastic energies of the cable, $E_i(t) = \int_0^t F_{yi}(t) \dot{\alpha}_i(t)\, dt$ is the input energy, and $E_c(t) = E_{ec}(t) + E_{dc}(t)$ is the SMA energy, including elastic energy $E_{ec}(t)$ and dissipative (hysteretic) energy $E_{dc}(t)$. Maximizing $E_{dc}(t)$ leads to the maximum damping force generated by the SMA.

$$f_c(t) = E\pi D_{SMA}^2 \left( \frac{v(x_c, t)}{L_{SMA}} - z\varepsilon_L \mathrm{sgn}(\varepsilon) \right) \tag{33}$$

where, $E$ is the modulus of elasticity, $v(x_c, t)$ is the cable transverse displacement at location $x_c$, and $L_{SMA}$ and $D_{SMA}$ are the length and the wire radius of SMA, respectively. According to Eq. (33), in order for $f_c$ to reach its maximum value, the term inside the parentheses must also be maximized. In that case, $z = 1$, leading to $\varepsilon = \frac{v(x_c,t)}{L_{SMA}} = \varepsilon_{max}$. Therefore, the condition for optimizing the SMA device length is defined by the relationship:

$$\varepsilon_{max} = \varepsilon_f^{AM} \tag{34}$$

where $\varepsilon_f^{AM}$ is the strain corresponding to the stress at the end of the martensite transformation. Consequently, the optimal length of the SMA device is determined by:

$$L_{SMA}^{opt} = \frac{|v^{max}(x_c, t)|}{\varepsilon_{max}} \tag{35}$$

Moreover, based on Eq. (33), the radius of the SMA wire in the SMA device should be selected as large as possible.

To examine the damping effectiveness of the SMA device in all three natural vibration modes, the geometry and properties of the stay cable are given in Table 1.

*Table 1.* Geometric properties of the stay cable model [21].

| Parameter | Symbol | Value | Unit |
|---|---|---|---|
| Cable length | $L$ | 55.4 | m |
| Mass per unit length | $m$ | 44 | kg/m |
| Inclination angle | $\theta$ | 16.5 | deg |
| Elastic modulus | $E_c$ | 19e10 | $\mathrm{N/m^2}$ |
| Cross-sectional area | $A_c$ | 55.5e-4 | $\mathrm{m^2}$ |
| Static tension | $T$ | 4313.5e3 | N |

The formula commonly used to calculate the deflection of a stay cable is: $d = \frac{mgL^2 \cos\theta}{8T}$.

In the case of the Rades-La Goulette cable-stayed bridge [21], the tension in the stay cable is $T = 4313$ kN, which results in a deflection of $d = 0.043$ m. It is clear that when the cable is fitted with a damper, its oscillation amplitude is reduced compared to when it is not equipped.

Thus, $d > v^{max}$. To calculate the optimal length of the SMA damper, we fixed the installation position of the damper at $0.1L$. The strain $\varepsilon_f^{AM}$ and the material properties of the SMA are provided in Table 2. The maximum transverse displacement $v^{max}(x_c, t)$ is selected as 0.03 m, ensuring that it is less than the transverse displacement at the mid-span of the cable. The diameter of the SMA wire is chosen to be $D_{SMA} = 20$ mm. Based on these parameters, the optimal length of the SMA is determined using Eq. (35) to be $L_{SMA}^{opt} = 0.46$ m.

*Table 2.* Material parameters [22].

| $E_A$ (Mpa) | $E_M$ $(Mpa)$ | $\sigma_s^{AM}$ $(Mpa)$ | $\sigma_s^{MA}$ $(Mpa)$ | $E$ $(Mpa)$ | $\varepsilon_f^{AM}$ (%) | $\tau$ | $H$ $(Mpa)$ | $I$ $(Mpa)$ | $G$ $(Mpa)$ | $\varepsilon_L$ (%) |
|---|---|---|---|---|---|---|---|---|---|---|
| 40000 | 20000 | 200 | 200 | 20000 | 6.5 | 1 | 7 | 14 | 0.2 | 5 |

With the above parameters and the calculated optimal length, the damping performance of the SMA device is demonstrated in Figure 3, which presents the cable response in its first three natural vibration modes. Figure 3 shows the transverse displacement $v(x_c, t)$ over time and the corresponding force response $f_c$ as a function of $v(x_c, t)$. The left plot shows the variation of the transverse displacement across the three vibration modes over time. In the first vibration mode, the amplitude decays more slowly than in the second and third modes, indicating higher energy dissipation in the higher modes. Because the frequency of mode 3 exceeds that of mode 2, which in turn surpasses mode 1, faster energy dissipation occurs. This observation is reinforced by the right plot, which depicts the relationship between force $f_c$ and displacement $(x_c, t)$. The first mode has the lowest force, while the second mode, and especially the third mode, exhibit significantly higher forces, suggesting that the SMA damper generates stronger force responses in the higher vibration modes. This reflects the nonlinear characteristics of the SMA damper, where the force response level varies according to each vibration mode.

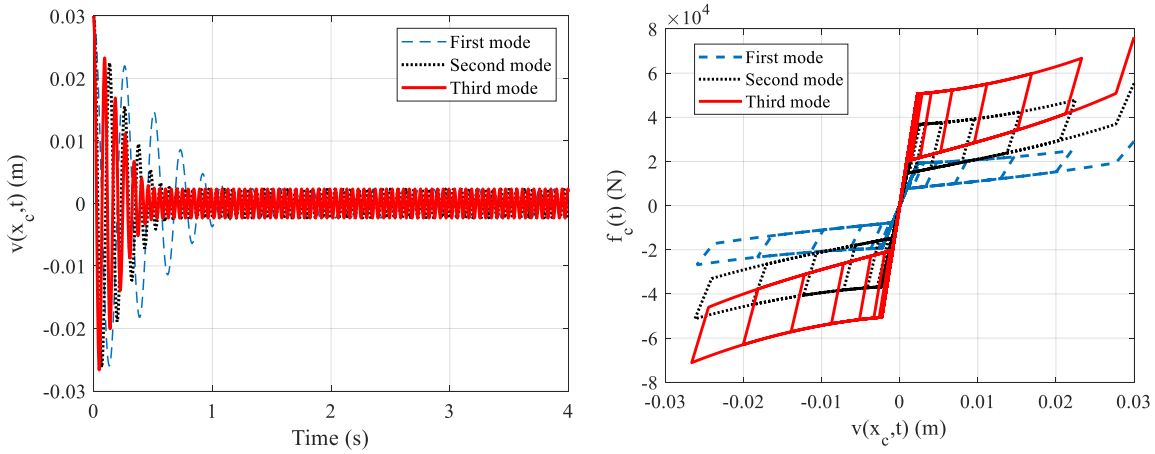


*Figure 3.* Dynamic response of the cable's three vibration modes.

To further emphasize the advantages of the proposed two-floor SMA damper, a comparison is made with the traditional tuned mass damper (TMD), a well-established solution for vibration control in cable-stayed bridges. In the study by Ben MekkiAuricchio [18], the TMD was installed at the mid-span of the cable and optimized using a mass ratio of 5 % to target a specific natural mode. The time-history responses, illustrated in Figures 4 to 6, demonstrate that the SMA damper consistently provides faster attenuation of vibration amplitudes and shorter stabilization times across all modes.

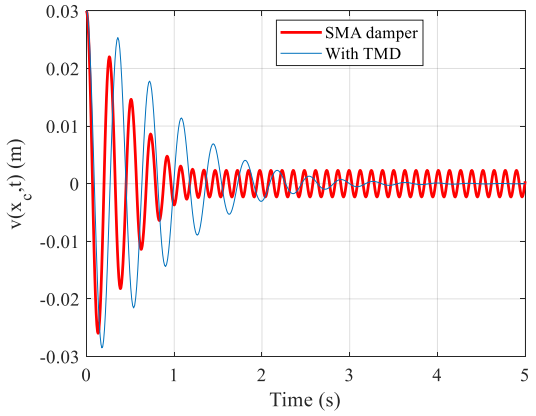


*Figure 4.* Comparison between the SMA damper and the TMD in controlling the free vibration of the stay cable in the first mode.

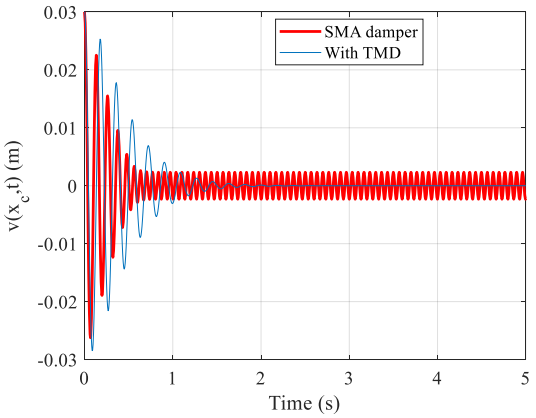


*Figure 5*. Comparison between the SMA damper and the TMD in controlling the free vibration of the stay cable in the second mode.

Quantitatively, the SMA damper reduces the maximum displacement by approximately 50–60% compared to the TMD across all modes, while also achieving a notably shorter stabilization time. In the first mode, the SMA-controlled cable stabilizes in less than 1.5 s, whereas the TMD requires longer, indicating higher effective damping due to the SMA's hysteresis and phase transformation behavior. This advantage persists in higher modes: in the second mode (Figure 5), the SMA damper suppresses oscillations faster with lower peak amplitude, and in the third mode (Figure 6) it maintains a compact, stable vibration profile while the TMD response remains more prolonged. Although the TMD may attenuate small-amplitude free vibrations more effectively, the SMA damper consistently provides stronger and faster vibration control across the examined modes.

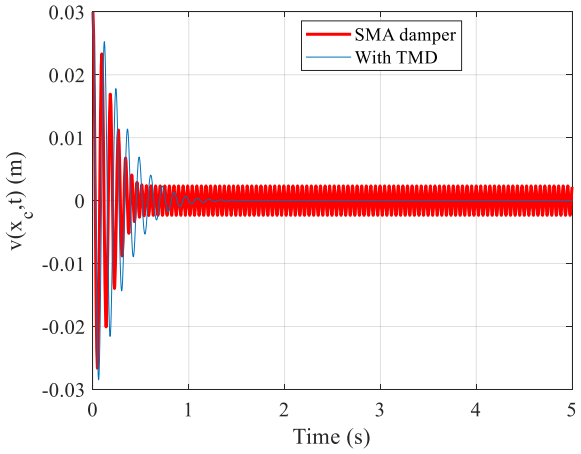


*Figure 6.* Comparison between the SMA damper and the TMD in controlling the free vibration of the stay cable in the third mode.

In addition to evaluating performance, the influence of design parameters on damper efficiency is also examined. The relationship between the SMA diameter, damper installation position, and optimal force $f_c$ is shown in Figure 7.

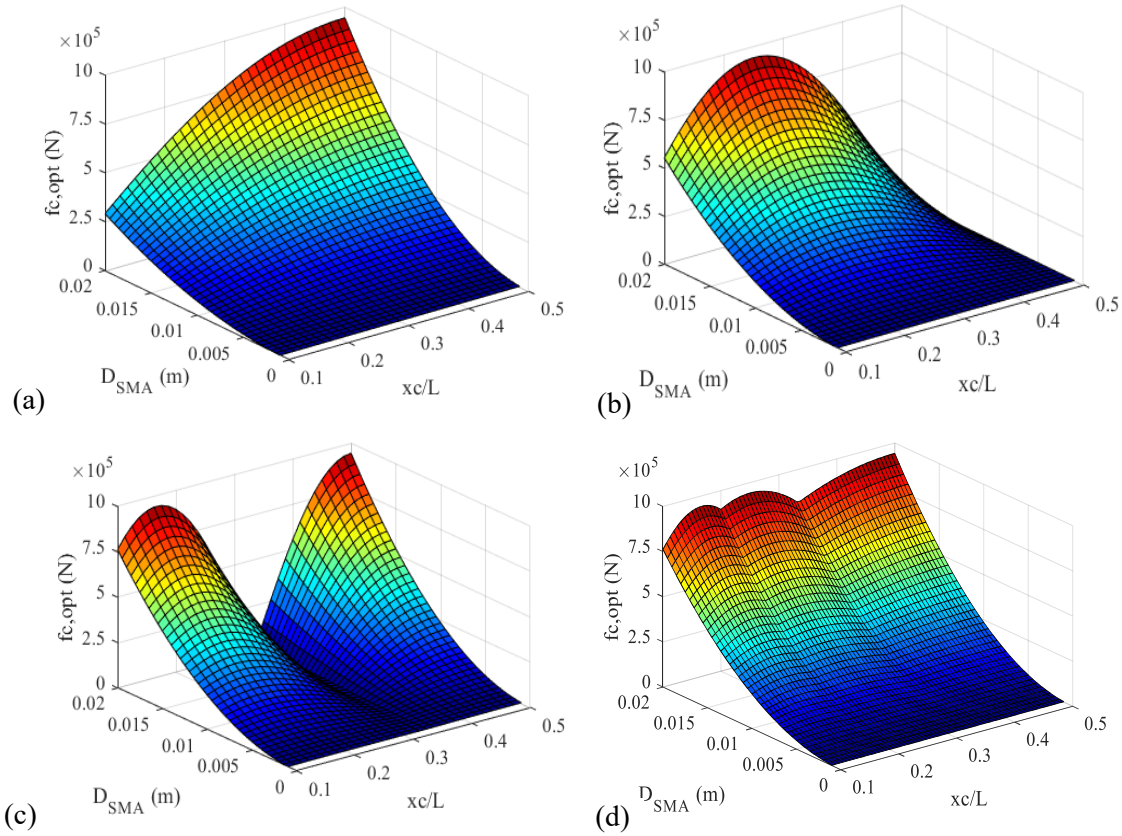


*Figure 7.* Relationship between diameter, position and force $f_c$: (a) First mode, (b) Second mode, (c) Third mode, and (d) Combination of three modes.

Figure 7 illustrates the relationship between the SMA diameter ($D_{SMA}$), the damper installation position ($x_c/L$), and the optimal force $f_{c,opt}$ across three vibration modes of the cable, along with a combined plot for all three modes. In the first mode (Figure 7(a)), $f_{c,opt}$ increases significantly as $D_{SMA}$ increases and the installation position moves closer to the mid-span, indicating that the best damping effect is achieved when the damper is placed at the mid-span with a larger SMA diameter. For the second mode (Figure 7(b)), $f_{c,opt}$ also increases with a larger $D_{SMA}$ and reaches optimal damping performance when the damper is installed near a quarter-span position, suggesting that this is the ideal location for the second mode oscillations. In the third mode (Figure 7(c)), $f_{c,opt}$ similarly rises with an increasing $D_{SMA}$, with the best damping effect observed when the damper is installed at either a sixth-span or mid-span position. For each vibration mode, the plots enable engineers to efficiently calculate the optimal damping force required to reduce vibrations in the cable-stayed bridge cables, using the available parameters. The combined plot (Figure 7(d)) incorporates the effects of all three oscillation modes, showing regions where $f_{c,opt}$ reaches its maximum. This diagram also indicates that the maximum damping force can be easily determined from parameters $D_{SMA}$ and $x_c/L$ to enhance the damper's vibration reduction capability in cases where the cable is subjected to all three vibration modes. This insight is crucial for the practical installation of dampers on stay cables, helping to optimize costs, ensure effective damping, and enhance the longevity of bridge structures.

## 5. CONCLUSIONS

This study presented a passive two-floor damper based on the superelastic effect of SMA to control vibrations in cable-stayed bridge systems. The two-floor damper was designed to maximize energy dissipation and ensure full deformation recovery after each vibration cycle, thereby enhancing cable stability and extending the service life of the bridge. Additionally, we proposed a simplified constitutive model that accurately simulates the superelastic effect of SMA, meeting the requirements for structural engineering applications. Using this model, we derived the dynamic equations to describe the cable's response when the damper is applied across different natural vibration modes. The results indicate that the two-floor SMA damper achieves high effectiveness in reducing cable oscillation amplitudes, outperforming a conventional tuned mass damper in both peak displacement reduction and stabilization time, particularly in higher vibration modes where energy dissipation is crucial.

We also optimized the length and diameter of the SMA wires to achieve maximum energy dissipation and developed charts illustrating the damping efficiency of the two-floor SMA damper according to installation position and wire diameter across three vibration modes of the cable in cable-stayed bridges. These charts assist in selecting the optimal installation position in practice to ensure high damping efficiency, while also providing feasible design guidance for real-world applications.

The two-floor damper concept with a simplified constitutive model not only optimizes damping performance but also simplifies the design and construction process, ensuring stability and durability for cable-stayed bridges. Future studies can focus on refining the configuration of the two-floor damper to further enhance vibration control, particularly for large bridge systems subjected to complex dynamic loads.

***Acknowledgements.*** This work was supported by VNU University of Engineering and Technology under project number CN24.22.

***CRediT authorship contribution statement.*** Hoang Ngoc Quy: Investigation, Writing – original draft, Writing – review & editing. Nguyen Van Duy: Software, Formal analysis, Writing – review & editing. TruongGiang Nguyen: Conceptualization, Methodology, Writing – review & editing, Supervision.

***Declaration of competing interest.*** The authors declare that there is no conflict of interest in this paper.

## REFERENCES

1. Xu Y. L., Zhu L. D., Wong K. Y., Chan K. W. Y. - Field measurement results of Tsing Ma suspension Bridge during Typhoon Victor. Struct. Eng. Mech., **10**(6) (2000) 545-559. https://doi.org/10.12989/sem.2000.10.6.545.
2. Matsumoto M., Shiraishi N., Shirato H. - Rain-wind induced vibration of cables of cable-stayed bridges. J. Wind Eng. Ind. Aerodyn., **43**(1-3) (1992) 2011-2022. https://doi.org/10.1016/0167-6105(92)90628-n.
3. Kareem A., Kline S. - Performance of Multiple Mass Dampers under Random Loading. J. Struct. Eng., **121**(2) (1995) 348-361. https://doi.org/10.1061/(asce)0733-9445(1995)121:2(348).
4. Spencer B. F., Nagarajaiah S. - State of the Art of Structural Control. J. Struct. Eng., **129**(7) (2003) 845-856. https://doi.org/10.1061/(asce)0733-9445(2003)129:7(845).

5. Xu Y. L., Xia Y. - Structural Health Monitoring of Long-Span Suspension Bridges. CRC Press, (2011). https://doi.org/10.1201/b13182.
6. Liu Y., van Humbeeck J. - On the Damping Behaviour of Niti Shape Memory Alloy. J. Phys. IV, **07**(C5) (1997) C5-519-C515-524. https://doi.org/10.1051/jp4:1997582.
7. Lagoudas D. C. - Shape memory alloys. Science and Business Media, LLC., (2008).
8. Pan Q., Cho C. - Proceedings of the 17th International Metallurgical and Materials Conference METAL, (2008)
9. Lv H., Huang B. - Parametric study of a new tuned mass damper with pre-strained SMA helical springs for vibration reduction. Smart Struct. Syst., **31**(1) (2023) 89-100.
10. Desroches R., Smith B. - Shape Memory Alloys in Seismic Resistant Design and Retrofit: A Critical Review of Their Potential and Limitations. J. Earthq. Eng., **8**(3) (2008) 415-429. https://doi.org/10.1080/13632460409350495.
11. Rajoriya S., Mishra S. S. - Application of SMA wire in vibration mitigation of bridge stay cable: a state-of-the-art review. Innov. Infrastruct. Solut., **7**(3) (2022) 192. https://doi.org/10.1007/s41062-021-00733-4.
12. Dolce M., Cardone D., Marnetto R. - Implementation and testing of passive control devices based on shape memory alloys. Earthq. Eng. Struct. Dyn., **29**(7) (2000) 945-968. https://doi.org/10.1002/1096-9845(200007)29:7%3C945::AID-EQE958%3E3.0.CO;2-%23.
13. Machado L. G., Savi M. A. - Medical applications of shape memory alloys. Braz. J. Med. Biol. Res., **36**(6) (2003) 683-691. https://doi.org/10.1590/s0100-879x2003000600001.
14. Helbert G., Dieng L., Arbab Chirani S., Saint-Sulpice L., Lecompte T., Calloch S., Pilvin P. - Investigation of NiTi based damper effects in bridge cables vibration response: Damping capacity and stiffness changes. Eng. Struct., **165** (2018) 184-197. https://doi.org/10.1016/j.engstruct.2018.02.087.
15. Huang H., Mosalam K. M., Chang W.-S. - Adaptive tuned mass damper with shape memory alloy for seismic application. Eng. Struct., **223** (2020) 111171. https://doi.org/10.1016/j.engstruct.2020.111171.
16. Hoang N. Q., Haidang P., Phan D. H., TruongGiang N. - Proceedings of the 11th National Conference on Mechanics, Vietnam Association of Mechanics, (2022) 474-484.
17. Auricchio F., Sacco E. - A one-dimensional model for superelastic shape-memory alloys with different elastic properties between austenite and martensite. Int. J. Non-Linear Mech., **32**(6) (1997) 1101-1114. https://doi.org/10.1016/s0020-7462(96)00130-8.
18. Ben Mekki O., Auricchio F. - Performance evaluation of shape-memory-alloy superelastic behavior to control a stay cable in cable-stayed bridges. Int. J. Non-Linear Mech., **46**(2) (2011) 470-477. https://doi.org/10.1016/j.ijnonlinmec.2010.12.002.
19. Rajoriya S., Mishra S. S. - International Symposium on Plasticity and Impact Mechanics, Springer Nature Singapore, (2022) 205-219. https://doi.org/10.1007/978-981-99-6255-6_18.
20. Irvine H. M. - Cable Structures. The MIT Press, Cambridge, MA (1981).
21. Soltane S., Mekki O. B., Montassar S. - Optimal Design of a Passive SMA Damper to Control Multi-modal Stay Cable Vibrations. J. Vib. Eng. Technol., **11**(3) (2022) 1343-1358. https://doi.org/10.1007/s42417-022-00644-3.
22. Fugazza D. - Use of shape-memory alloy devices in earthquake engineering: Mechanical properties, advanced constitutive modelling and structural applications. Doctoral dissertation Thesis, Università degli Studi di Pavia (2005).